



# Laser-powder bed fusion molds without post-processing for micro-injection molding of mini/micro-products

Rossella Surace<sup>1</sup> · Vito Errico<sup>2</sup> · Marcello Valori<sup>3</sup> · Irene Fassi<sup>3</sup> · Sabina Luisa Campanelli<sup>2</sup>

Received: 2 December 2022 / Accepted: 11 May 2023 / Published online: 17 May 2023  
© The Author(s) 2023

## Abstract

The use of additive manufacturing (AM) processes at the micro-scale helps to increase the development of micro-systems, thus enabling shorter tooling development to be exploited for other micro-technologies, such as micro-injection molding ( $\mu$ -IM). In recent years, these process combinations have shown their capability of providing greater flexibility to micro-technologies and facilitating a high production rate, in particular allowing  $\mu$ -IM to be economically feasible for low-volume production. Therefore, in order to assess the feasibility of micro-metal AM for  $\mu$ -IM mold production, a set of mini- and micro-polymeric parts injected by using molds realized via the laser-powder bed fusion (L-PBF) process is discussed in this paper. The molds were manufactured in low-carbon steel and have been characterized and tested experimentally, without any post-process treatment. Two selected geometries, corresponding to a mini dogbone for tensile tests and a flexural hinge with features at the micro-scale, were designed and realized by the  $\mu$ -IM process. These were replicated in order to assess the accuracy of the whole process. The obtained results of replication accuracy and mechanical tests confirm that the  $\mu$ -IM process, performed with an L-PBF-made mold insert, is feasible and affordable for micro-production, although great accuracy, especially in mold design, fabrication, and assembly, is required.

**Keywords** Additive manufacturing · Laser-powder bed fusion · Micro-injection molding · Steel molds · Replication accuracy

## 1 Introduction

At present time, there is a growing interest in additive manufacturing (AM) technologies and their integration into the process chain. In particular, the implementation of AM for tool production in micro-injection molding ( $\mu$ -IM) may introduce several advantages. First, the AM option could significantly reduce the need to fabricate expensive molding tools, especially for small series of customized products; this option would provide feasible and affordable parts in reduced production time [1]. Furthermore, with respect to mold realized by polymer-based AM as stereolithography, the mold duration and tool life become comparable to traditional mold obtained by subtractive manufacturing [2, 3].

The technological processes of AM were initially developed for plastic material processes mainly to enable rapid prototyping. Later, thanks to impressive technological progress, it was possible to extend their use to metallic materials and obtain direct production of metal parts. Metal AM (MAM) involves several processes that can differ in type, used energy source, and metallic material nature. Among the

---

✉ Rossella Surace  
rossella.surace@stiima.cnr.it

Vito Errico  
vito.errico@poliba.it

Marcello Valori  
marcello.valori@stiima.cnr.it

Irene Fassi  
irene.fassi@stiima.cnr.it

Sabina Luisa Campanelli  
sabinaluisa.campanelli@poliba.it

<sup>1</sup> Institute of Intelligent Industrial Technologies and Systems for Advanced Manufacturing, National Research Council, Via P. Lembo 38/F, 70124 Bari, Italy

<sup>2</sup> Department of Mechanics, Mathematics, and Management, Politecnico Di Bari, Via E. Orabona 4, 70126 Bari, Italy

<sup>3</sup> Institute of Intelligent Industrial Technologies and Systems for Advanced Manufacturing, National Research Council, Via A. Corti 12, 20133 Milan, Italy

different categories, the ISO/ASTM52900-15 [4] standard identifies the following main technologies: based on PBF (powder bed fusion), DED (directed energy deposition), and those based on SL (sheet lamination) [5]. By the use of the aforementioned processes and technologies, new design possibilities can be implemented, such as lightweight structures with inner lattice components or parts with complex geometries that are usually difficult and very expensive to reproduce with traditional technologies; an example is given by molds that contain internal conformal cooling channels without any design constraints [6–8]. Furthermore, the recent hybrid additive manufacturing (HAM), which integrates additive and subtractive manufacturing, has widened the range of component design and prototyping, such as for injection molds exhibiting high geometric freedom to produce parts with required characteristics; the implementation of HAM demonstrated about a 50% reduction in the injection molding cycle time and an increase of 30% in mold life [9].

In the plastic industry, metal additive manufacturing is mostly used for mold fabrication, although L-PBF, specifically, seems to be applied mainly in the macro-area, such as the automotive sector [10], rather than used for the production of smaller and/or micro-parts or features. Moreover, it is acknowledged that the optimization of conformal cooling channels has a paramount role in this macro-area. Molds can feature internal cooling channels yielding uniform and rapid cooling of the component before its removal and thus improve production quality and efficiency [6, 11, 12]. Indeed, this solution is not required at the micro-scale due to the fast cooling experienced by polymers in the micro-injection molding process, since the surface-to-volume ratio is much higher than typical values characterizing conventional injection molded products. Therefore, high injection speed and high mold temperature have to be used to prevent premature solidification, and cooling channels are not requested, differently from traditional injection molding, in which they are of paramount importance.

In this context, several works in the literature demonstrated the feasibility and desirability of making injection molds by means of L-PBF and hybrid technologies obtained by the integration of L-PBF and conventionally manufactured (CM) processes [13]. Specifically, Saby et al. [14] studied the L-PBF printability of IM mold considering three different steels: maraging stainless steels, martensitic stainless steels, and non-stainless martensitic steels. The results showed that the as-built stainless steels (PM420, X15TN, L40, and CX) display interesting characteristics in terms of mechanical properties and surface performance, and, as such, these materials are eligible to be used as an alternative to the frequently used 18Ni300 steel. Tan et al. [15] explored the feasibility of L-PBF technology and fabricated an injection mold having self-supporting wide conformal cooling

channels. The experimental results and numerical simulations revealed improvements in the producibility, cooling efficiency, and throughput of the new conformal cooling mold produced via L-PBF. Sinico et al. [16] conducted a topology optimization on an injection mold insert produced via L-PBF technology. The study was carried out with both commercial software (topology optimization (TO)) and in-house TO software. The results show that the new in-house TO tool, which provides ad hoc thermal constraints, reduces the possibility of heat accumulation. The absence of localized overheating in the optimized mold made it possible to achieve improved geometric accuracy and surface characteristics.

Samei et al. [9] conducted a study aimed at the possibility to produce a component by combining AISI 420 casting and Corrax (a maraging stainless steel grade) L-PBF. In particular, hybrid molds having complex geometries, reinforced surfaces, and higher corrosion resistance were successfully produced.

However, when micro-mold manufacturing, and in particular its fabrication via L-PBF technology, is examined, few studies can be found in the current literature [17]. In fact, the main drawback to realizing micro-molds with AM is the poor surface finish, usually requiring a further post-processing phase by additional machining [1, 18]. In this regard, two studies on mold manufacturing for the  $\mu$ -IM process which involved further processing downstream of the print are proposed by Qian et al. [19] and Schubert et al. [20]. In particular, Qian et al. presented a work in which an electric discharge micro-machining technique was used to obtain molds for micro-components, with good results in terms of production time and shape accuracy. Moreover, Schubert et al. shaped molds through an electrochemical process, i.e., continuous electrolytic free jet (Jet-ECM), achieving the high precision required by  $\mu$ -IM. A recent paper [21] analyzes the current possibilities and limitations of MAM for plastic injection molding tool applications, demonstrating the opportunity to limit post-processes to heat treatment and machining only when required to ensure assembly.

In the present work, the feasibility of the L-PBF/ $\mu$ -IM process chain has been evaluated by designing and fabricating mold inserts for mini-/micro-component production (Fig. 1). The molds were manufactured in low-carbon steel, e.g., 18Ni300 maraging steel, and their dimension and surface quality have been characterized and tested experimentally. The molds were directly applied as built from L-PBF without any further post-processing. Two selected geometries, corresponding to a mini dogbone for tensile tests and a micro-flexural hinge, were designed, as they can represent a challenge from both L-PBF and  $\mu$ -IM manufacturing viewpoints. After the evaluation of the replication capability of samples, the obtained results confirmed that

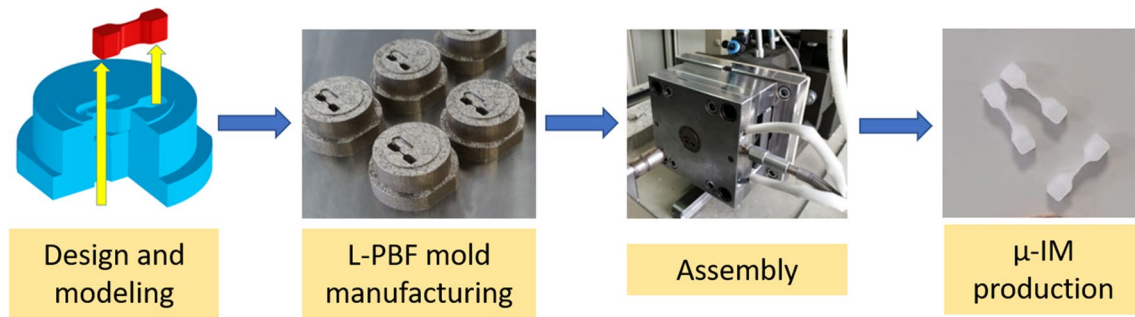


**Fig. 1** Process chain steps: mold design and modeling, L-PBF mold manufacturing, mold assembly, and final injection molding product

the  $\mu$ -IM process, performed with an L-PBF mold insert, is feasible and affordable, although special attention is devoted to preserving great accuracy, especially in mold design, fabrication, and assembly steps. Finally, functional tests (mechanical characterization) and geometrical and surface characterization were performed, confirming the possibility of using AM metal powders for mini- and micro-mold fabrication.

## 2 Part and mold design

The mold is composed of two parts: the block mold, which is the main part equipped with all subsystems (cooling, ejection, injection, hot distribution, etc.), and the mold insert with shaped cavities and melt distribution (cold runners). Typically, both mold block components and inserts are fabricated by traditional processes, and their manufacturing requires careful process design and machining time. In this work, the mold insert is easily replaceable and fabricated using L-PBF technology.

As a first case study, a dogbone sample suitable for micro-tensile tests was selected. The part thickness is 1 mm, and other dimensions are illustrated in Fig. 2. During mold design, in order to eject the part from the mold more easily, a draft angle was added to the vertical walls to avoid the high

friction of the part with the mold. In this regard, a previous study showed that when the same mold is manufactured by conventional technology (micro-milling, for instance), a draft angle of  $0.5^\circ$  is sufficient to apply damage control to the ejected parts [22]. However, due to the higher surface roughness of the mold fabricated via the L-PBF process, this draft angle value was unsuitable for intact part ejection. Thus, by also following the guidelines given in [23], during the design phase and subsequent fabrication, the draft angle was increased from 1 to  $2^\circ$  to accomplish correct part ejection.

The second case study proposes a flexural hinge (FH) part, which is a short flexible element having the function of a joint in flexure-based compliant mechanisms, where stocky parts behave as rigid links [24]. The FH based on a corner-filleted contour has been designed, and the dimensions are reported in Fig. 3. Since the hinge flexion angle is mainly affected by the geometry of the central stem, the target of the design has been the definition of the stem length (0.5 mm) and thickness (4 mm) in compliance with the manufacturing constraints [25]. This is the most challenging micro-feature of the part due to the high aspect ratio (high thickness in combination with a very thin width). In this case, the adhesion of the part on the mold surface is very tight and is more influential than in the dogbone specimen. Hence, different draft angles, increasing up to  $3^\circ$  ( $0.5-1-2-3^\circ$ ) were applied to favor the part ejection. Consequently, as the thickness

**Fig. 2** Dogbone test part: mold insert and part (a) and part design (mm) (b)

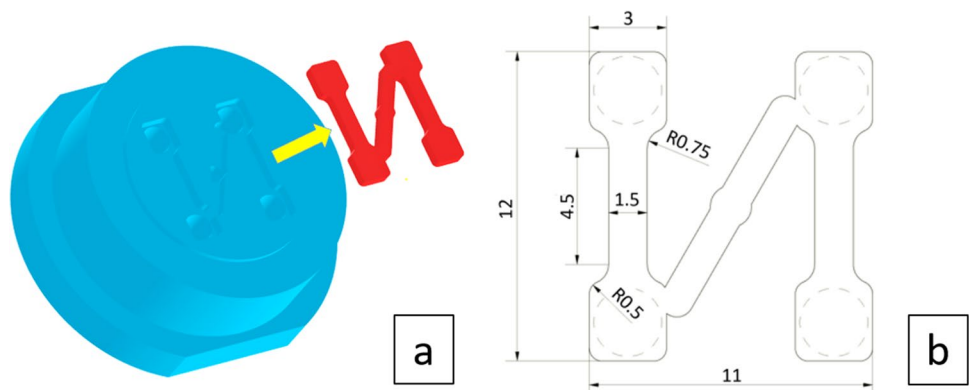


**Fig. 3** Flexural hinge test part: mold insert and part (a) and part design (mm) (b)

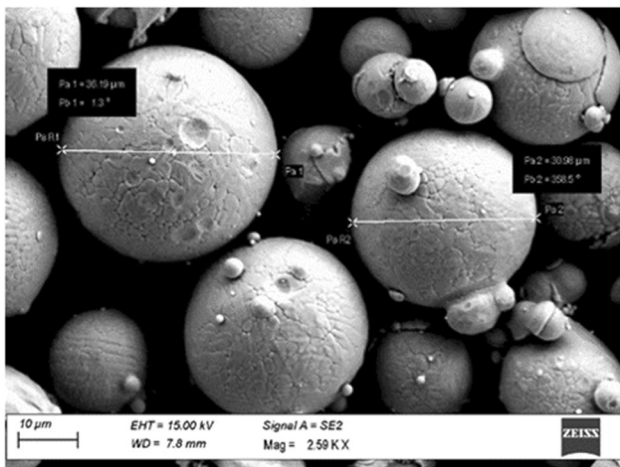
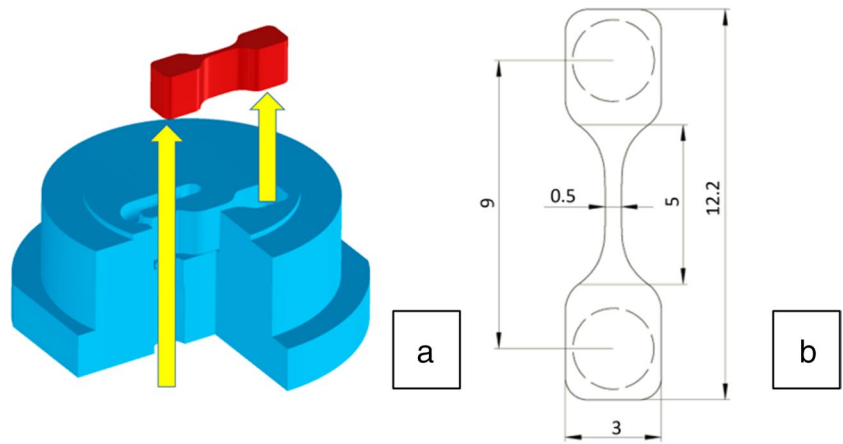


**Fig. 4** Scanning electron microscope (SEM Zeiss Sigma 300 VP) image of the 18Ni300 maraging steel powder, showing the shape and average size of the particles

of the part is 4 mm, the real dimensions in the bottom and upper planes of the mold were slightly different from the nominal ones, and the zero plane was set in the middle of the part thickness.

### 3 Mold manufacturing via laser-powder bed fusion process

A spherical-shaped powder of gas-atomized 18Ni300 maraging steel (Fig. 4) was used to manufacture the mold samples. Specifically, its size and chemical composition are shown in

Table 1. The chemical composition of the powder, obtained by inductively coupled plasma optical emission spectroscopy, was provided by the manufacturer of the AM system (GE Additive).

The designed molds, described in Section. 2, were manufactured by using the laser-powder bed fusion process. Specifically, a commercial M1 cusing machine made by concept laser (GE Additive) was used; the main AM machine characteristics are listed in Table 2.

Table 3 shows the manufactured mold inserts with the different tested draft angles (3 inserts fabricated for the dog-bone specimen and four inserts for the hinge). The process parameters used for fabrication are listed in Table 4; the parameter values are optimized and retrieved from results from previous work carried out on the same powder material [26]. The adopted scanning strategy is different for hinge molds (contour-infill and only infill) and for dogbone molds (only infill). However, the contour strategy used for hinges was then discarded due to unsatisfactory dimensional design

**Table 2** Concept laser M1 cusing machine characteristic

Technical data	M1 cusing
Build envelope (mm)	120 × 120 × max 200 (x, y, z)
Min. layer thickness (μm)	20
Type of laser	Diode-pumped solid-state laser–Nd: YAG
Laser wavelength (nm)	1064
Inert gas supply and consumption	N <sub>2</sub> – 5 l/min < 1 m <sup>3</sup> /h
Laser power (Watt)	100 (cw)
Laser spot diameter (μm)	200

**Table 1** Chemical composition according to the test method: ASTM E1479-16–ASTM E2594-20

Powder material	Range of particle size (μm)	Ni	C	Mo	Co	Ti	Fe
18Ni (300) maraging steel	15–53	18.7	0.02	3.73	10.4	1.15	Bal

**Table 3** Fabricated mold inserts

Specimen	Notation	Draft angle (°)			
		I	II	III	IV
Hinge	H	0.5	1.0	2.0	3.0
Dogbone	D	0.5	1.0	2.0	-

**Table 4** Printing process parameters

Process parameter	Unit	Value
Laser power	Watt	100
Exposure speed	mm s <sup>-1</sup>	180
Hatch distance	µm	140
Slice thickness	µm	30

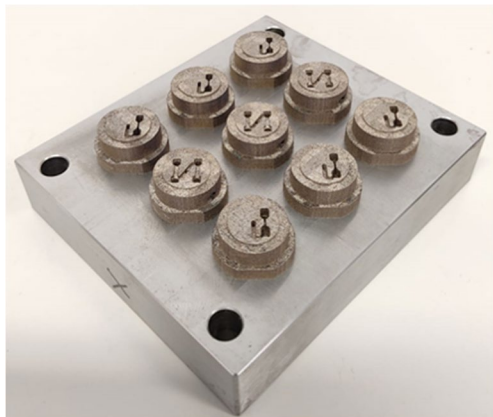
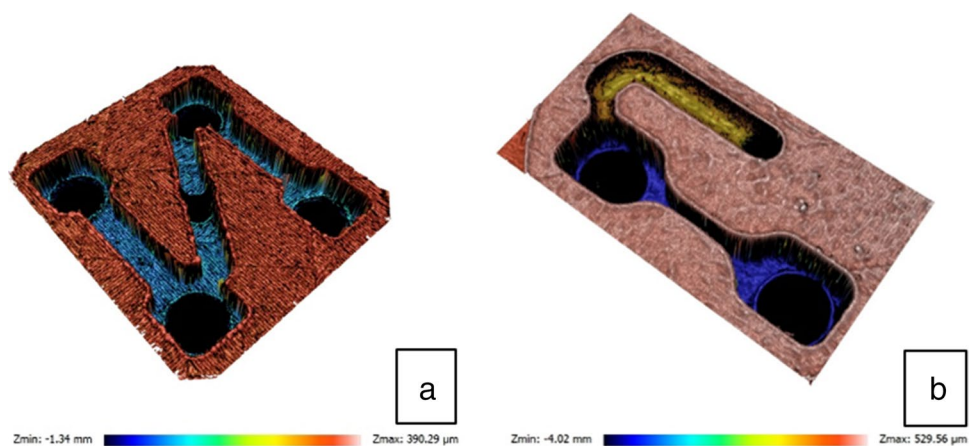


**Fig. 5** Example of the inserts manufactured by means of laser-powder bed fusion process positioned on the machine platform

**Fig. 6** Confocal images of two insert cavities: D0.5 (a) and H1.0 (b)



tolerances (as shown in the following section). Finally, the adopted scanning strategy involved random scanning islands of 5 × 5 mm<sup>2</sup> size. Indeed, this scanning approach and island size provide the combination generating the lowest residual

stresses on parts, as suggested by the available literature [27, 28]. Based on these considerations, this approach was specifically chosen to cope with fitting problems encountered during the mold insert assembly on the mold block. The identification of the molds was  $Tn$ , where  $T$  is the type of mold insert (H, hinge; D, dogbone) and  $n$  is the draft angle value. Figure 5 shows some of the fabricated molds.

### 4 Mold characterization

In order to compare the real dimensions of the two cavities realized in the molds with the nominal ones, the L-PBF mold inserts, separated from the building platform, have been dimensionally characterized by confocal microscopy (Zeiss Axio CSM 700, objective magnification × 10, spatial resolution 0.9 µm, z resolution 2 µm) and confocal-focus variation microscope (Sensofar Sneox3D optical Profiler, objective magnification × 20, spatial resolution 0.37 µm, z resolution 0.008 µm). Figure 6 shows the confocal images of two insert cavities (D0.5 and H1.0). The average values of the dimensions and corresponding standard deviations, along with nominal ones, are reported in Table 5 (dogbone) and 6 (flexural hinge). As inferable from both tables, the measured dimensions have very close values to the nominal ones. These results confirm the effectiveness and accuracy of L-PBF technology in the fabrication of molds with thin cavities.

Furthermore, based on dimensional measurements of dogbone and hinge inserts (see Tables 5 and 6 for reference), the geometric accuracy  $A$  has been calculated as the difference between the two corresponding measurements real “ $R$ ” and nominal “ $N$ ” for length, width, and thickness

respectively (Eq. 1):

**Table 5** Dogbone mold: nominal and real dimensions of the three inserts

D	Length (mm)	Width (mm)	Thickness (mm)
Nominal	12	1.5	1
D0.5	11.90	1.54	1.02
D1.0	11.99	1.52	1.03
D2.0	12.03	1.51	1.04

**Table 6** Flexural hinge mold: nominal and real dimensions of the four inserts

D	Length (mm)	Width (mm)	Thickness (mm)
Nominal	12.2	0.5	4
H0.5	12.25	0.51	4.07
H1.0	11.98	0.52	3.97
H2.0	12.11	0.51	4.04
H3.0	12.24	0.48	4.02

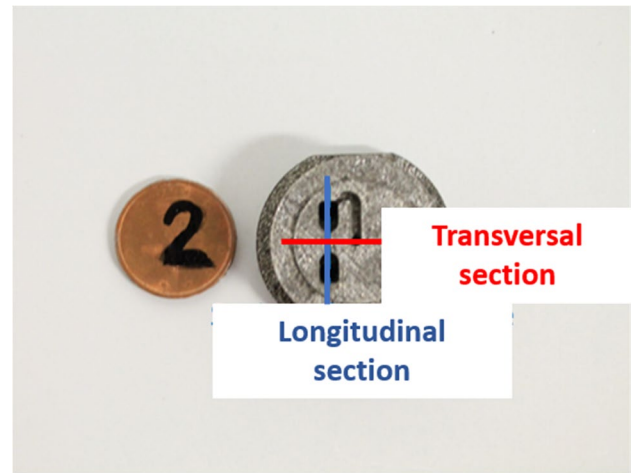
**Table 7** Inserts geometric accuracy

Insert	Geometric accuracy (%)
D0.5	1.83
D1.0	1.47
D2.0	1.64
H0.5	1.39
H1.0	2.19
H2.0	1.25
H3.0	1.44

$$A = \left( \frac{R - N}{N} \right) \times 100 \quad (1)$$

Then, the mean values of the measurements have been calculated for each insert, and the results provide the geometric accuracy of the inserts as shown in Table 7. The obtained accuracy range is 1.2–2.2%.

The narrow region of FH was the most demanding part for both technologies, L-PBF and  $\mu$ -IM, due to the high surface-to-volume ratio. Especially for the  $\mu$ -IM, the grasp effect of the mold wall could be very effective during sample ejection, while it represented a challenge for a cavity realized by metal AM. Therefore, two H inserts have been sectioned in the longitudinal and transversal directions of the channel for inner dimensional measurements and surface acquisition of the mold lateral wall (Fig. 7). The roughness value ( $R_a$ ) of the cavity, measured via the confocal microscope (acquisition length 3.5 mm, objective magnification  $\times 100$ , z resolution 0.2  $\mu\text{m}$ ) is  $5.8 \pm 0.02 \mu\text{m}$ . This value can be considered successful

**Fig. 7** Flexural hinge mold characterization by longitudinal and transversal sections of the narrow central feature for precise roughness and dimensional acquisition

for the L-PBF process applied for micro-manufacturing. Furthermore, the roughness of a D insert was acquired in the same way on the bottom surface, showing a value of  $7.9 \pm 0.05 \mu\text{m}$ .

From the transversal section (Fig. 7) and from the acquisition and magnification of the hinge thin feature (Fig. 8), it was possible to verify the inclination of the walls and thus the actual draft angle. The dimensions (top and bottom, width and depth) of the channel were acquired three times each: on the top, the mean width is 439  $\mu\text{m}$ , on the bottom is 404  $\mu\text{m}$ , and the depth is 3998  $\mu\text{m}$ . From these results, the calculated draft angle is  $0.5^\circ$  as expected. The widths both on the top and bottom are smaller than the design values; this was due to the chosen contour strategy, causing the decrease in dimensions. For this reason, the mold inserts were then produced with only an infill strategy.

## 5 Products manufacturing via a micro-injection molding process

The inserts were then mounted on the mold block and assembled in the micro-molding machine (Fig. 9a). In some cases, the assembly required little adjustments (fine sandpaper machining) to ensure the correct part fitting, especially between the ejector pins and the corresponding holes as mentioned in Section. 4 (Fig. 9b). In fact, all ejector holes were smaller than the nominal measure, especially the central one that is the smallest. No post-process was performed on the cavities to be injected, leaving them as built from the L-PBF process.

**Fig. 8** Confocal image of the transversal section of the hinge narrow central feature



The polymer polyoxymethylene (POM) (BASF Ultraform), belonging to engineering thermoplastics, has been chosen for this study. It has a partially crystalline structure with a high degree of crystallization depending on process parameters, and it presents an ideal combination of strength, stiffness, and toughness. These characteristics, in association with good tribological properties, make POM very suitable

for molding and critical engineering applications. Its main physical and mechanical properties are reported in Table 8. The material has been dried before use for 4 h at a temperature of 80 °C as suggested by the manufacturer.

The injection molding process was performed by the DesmaTec FormicaPlast 1 K machine, in which two units can be distinguished: the injection unit and the clamping one. The first consists of a hopper, a 6 mm piston to plasticize the material, and a 3 mm piston for the injection step. During this phase, the plastic pellets become a homogeneous melt as they progress through feeding, melting, compressing, and injection steps. This unit is also responsible for the control of the switchover position from the speed control of the process to the pressure one. The clamping unit guarantees the opening and closing of the mold, ensuring enough strength to withstand the force generated during the injection phase and, thus, preventing flash formation in the pieces.

The screening phase, for defining process parameters, was carried out for both features to control the production process and to fill the cavities completely. Initially, they were fixed starting from previous experimentation for similar features [25, 29] and then calibrated. In this way, it is possible to identify the technological operative window for the different couple material parts. Table 9 reports the levels of parameters for molding dogbones and flexural hinge parts.

For the hinges, the mold temperature set was slightly higher than the one used for the dogbones; this option aims at the prevention of rapid material condensation, which may occur on the narrow tool surface due to the high volume-to-surface ratio. For the same reason, and also considering the wall roughness, the holding pressure and time are decreased for hinge injection since these parameters are strictly related to shrinkage and warpage in thin-walled parts. Also, for the hinges, a mold release agent was used to favor extraction. After machine stabilization, samples were collected for characterization. Figure 10a, b shows injected dogbones and hinge samples.

## 6 Parts characterization and results

The dogbone samples, realized by inserts with different draft angles, were successfully molded and dimensionally characterized to verify the replication accuracy and hence the potentiality of this approach.

For each realized insert, almost one hundred injection cycles were performed, and then the insert was dismantled and observed by visual and microscope inspection to verify the absence of wear damage or cracks as found. Differently, in a previous study, by using a similar insert realized by SLA [25], only a small batch of about 10–15 samples was realized by means of a single printed mold before a crack forms near the gate.

**Fig. 9** Insert assembly on the machine mold block (a) and verification of ejector pinhole fitting (b)

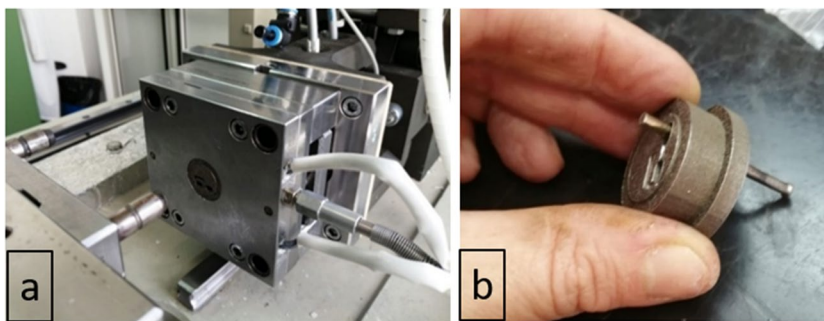


**Table 8** POM material properties

Name	Trade name	Grade	Manuf	MVR (cm <sup>3</sup> /10 min)	Density (kg/m <sup>3</sup> )	Tensile modulus (Mpa)
POM	Ultraform	N2320 003	Basf	7.5	1400	2700

**Table 9** Injection molding process parameters

Parameter	<i>D</i>	<i>H</i>
Melt temperature (°C)	230	230
Mold temperature (°C)	80	100
Injection velocity (mm/s)	150	150
Holding pressure (MPa)	1000	800
Holding time (s)	3	2
Cooling time (s)	5	5
Run (mm)	12.5	15

The average values and standard deviations of the ten dogbone samples are reported in Table 10. They were randomly chosen in the produced batch after the machine

reaches regime conditions [29]. Then, the length, width, and thickness of the produced parts are measured and compared to the cavities' dimensions. The obtained values are lower than the real dimensions of the cavity (Table 5), but the differences are in the range of 0–2%, which is acceptable considering the level of POM shrinkage (2.1%, ISO 294–4). The geometric accuracy was evaluated once again by comparing the mean value of the measured samples with each insert using Eq. 1, in which *R* is the cavity's real dimensions and *N* is the specimens' measurements.

Furthermore, tensile tests were performed using a Shimadzu EZ-S dynamometer equipped with a 500 N load cell and pneumatic grippers. Three samples, produced by each mold and belonging to the ten measured parts, have been tested at 1 mm/min according to ISO 527 standards. The

**Fig. 10** Dogbone (a) and hinge (b) injected samples

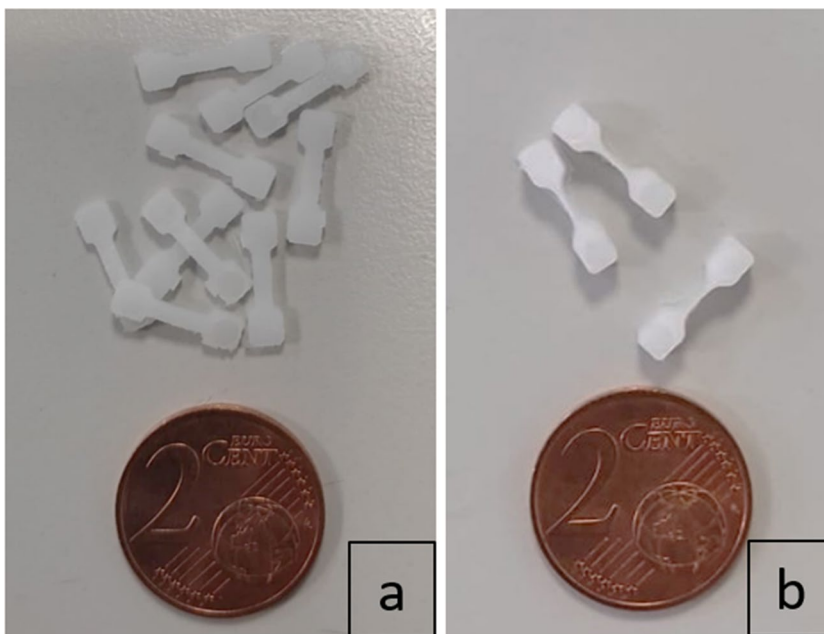




**Table 10** Dogbones: dimensional characterization and geometric accuracy

D	Length-L (mm)	Width-W (mm)	Thickness-T (mm)	Geometric accuracy (%)
D0.5	11.9±0.06	1.51±0.05	1.04±0.03	1.3
D1.0	11.92±0.02	1.57±0.02	1.05±0.02	1.9
D2.0	12±0.11	1.59±0.04	1.04±0.02	1.8

nominal stress was evaluated by dividing the recorded load by the initial cross-section of the specimen; the nominal strain was evaluated by dividing the crosshead displacement by the initial length of the narrow central section of the specimen. Typical nominal stress vs. nominal strain curves obtained for each examined specimen is reported in Fig. 11; a pretension load due to micro-specimen clamping causes a shift in the curves (the starting point is not zero). As inferable from the results of the three inserts (D0.5., D1.0, and D2.0), the specimens exhibit a ductile behavior due to the highly experienced elongation. Table 11 reports the numerical results.  $E_{tg}$  in the table represents the tangent modulus, i.e., the slope of the stress–strain curve in the linear range, and thus is equal to Young’s modulus. This parameter is suitable to characterize the behavior of materials that have been stressed beyond the elastic region. Generally, the tangent modulus can have different values depending on the point at which it is determined.

Furthermore, in a previous work by the authors, a dogbones’ production has been carried out made of the same polymeric material (POM). Those samples were fabricated via a traditionally manufactured steel mold which was, successively, tested mechanically in the same conditions [30].

**Table 11** Dogbone sample mechanical properties

D	$E_{tg}$ (MPa)	Stress max (MPa)
D0.5	607.91 ± 36.70	62.92 ± 2.73
D1.0	646.26 ± 11.38	67.18 ± 0.14
D2.0	641.09 ± 40.37	65.73 ± 3.54

**Table 12** Dogbone mechanical properties from ref. [30]

Sample	Stress max (MPa)
POM1	62 ± 2
POM2	65 ± 3
POM3	68 ± 2
POM4	67 ± 4

In that research, the mold was realized by Ni–Cr–Mo steel and manufactured by micro-EDM with a draft angle of 0.5°. The maximum stress values measured for the four batches of tested samples (POM 1–4) are reported in Table 12 and compared with the values of the present research (Table 11). As inferable from the comparison of Tables 11 and 12, the stress max values of both dogbone samples are quite similar, confirming the functionality of these samples and thus the feasibility of additive-manufactured metallic mini-molds.

Successively, the hinge samples were successfully molded by using the three inserts with different draft angles (1°, 2°, and 3°) while the IM process of the feature with the insert having a draft angle of 0.5° was not completed due to ejection issues. The dimensional accuracy of the molded hinges (H1, H2, and H3) was investigated; the mean and standard deviation values of measurements related to ten randomly chosen samples are listed in Table 13. The dimensional

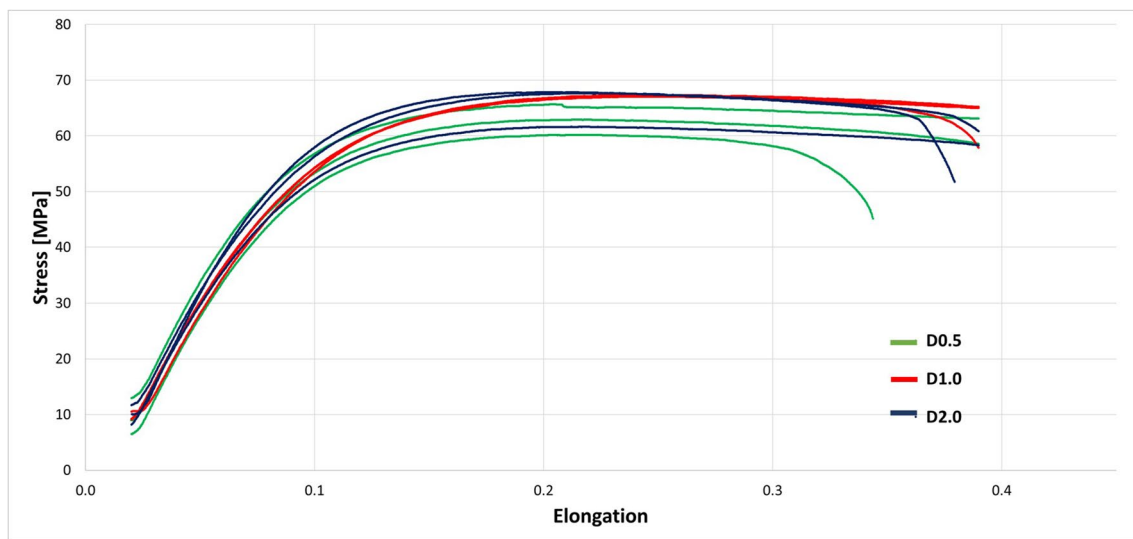


**Fig. 11** Stress vs. elongation for dogbone samples

accuracy of the injected parts is good, considering also the issue experienced during hinge production regarding the strong bond between the injected parts and mold walls; these effects, in some cases, resulted in the deformation of the central feature, as visible in Fig. 12. The difference between real mold and sample dimensions is higher for hinge parts than for dogbone samples (up to 5% for some measurements), especially in relation to the width of the narrow section. Thus, in this case, some corrections and alternative solutions can be found as secondary machining of the mold, for example sandblasting.

Regarding the roughness of the molded samples, the obtained values show wide dispersion around the mean values; for *D* samples, the roughness evaluated with the confocal microscope is  $7.7\ \mu\text{m}$  with a standard deviation of  $1.2\ \mu\text{m}$ , while for *H* samples are  $3.4$  with a standard deviation on  $1.1\ \mu\text{m}$ .

In previous work, the mechanical flexural response of FHs obtained by injection molding combined with SLA-manufactured molds was analyzed by authors in [25]. In that case, the components exhibited a linear mechanical response in a wide flexion range (up to  $60^\circ$ ), demonstrating the reliability of components realized with such a technology combination. The reasonable expectation is for an analog behavior from the FHs obtained by the process here described that differs slightly for hinge design.

## 7 Economic analysis

Beyond the quality of the molded specimen, the production time and cost were estimated and compared to evaluate the feasibility of the proposed integrated approach. This economic analysis aims to highlight the advantages of the implemented process chain aiming at decreasing time and cost for micro-injection molding tooling. The values reported in Table 14 were calculated considering the following costs: machine (micro-milling  $23\ \text{€}/\text{h}$ , micro-EDM  $40\ \text{€}/\text{h}$ , SLA  $0.7\ \text{€}/\text{h}$ , L-PBF  $30\ \text{€}/\text{h}$ ), materials ( $100\ \text{€}$  for bulk insert realized by turning and milling), and operator ( $40\ \text{€}/\text{h}$ ). Regarding the operators' time, the following values were considered: 2 h for milling, 1 h for EDM, 0.75 h for SLA, and 1.5 h for L-PBF. The cost and time for mold design

**Table 13** Flexural hinges: dimensional characterization

<i>H</i>	Length (mm)	Width (mm)	Thickness (mm)	Geometric accuracy (%)
H1.0	$11.79 \pm 0.06$	$0.55 \pm 0.03$	$4.04 \pm 0.03$	2.8
H2.0	$12.21 \pm 0.07$	$0.52 \pm 0.03$	$4.00 \pm 0.05$	1.3
H3.0	$11.97 \pm 0.08$	$0.51 \pm 0.06$	$4.02 \pm 0.03$	2.9



**Fig. 12** Example of the deformed part due to difficult ejection of the narrow part

were neglected because they were the same. The finishing of milling and micro-EDM has been evaluated for reaching the same roughness as L-PBF.

Through metal additive manufacturing (L-PBF), the production cost of the mold can be reduced by 53% compared to EDM, and it also provides a shorter manufacturing time. The reduction with respect to traditional milling is about 16%, even though the production time is higher. If the mold is entirely realized by SLA, it will request considerably lower costs than other processes. Still, it will be suitable only for small production series, as this polymeric mold is subjected to rapid failure. Moreover, the production time is relatively high.

## 8 Conclusions

This paper aims to contribute to the development of a process chain involving L-PBF and  $\mu$ -IM, in relation to the manufacturing of mini- and micro-polymeric parts. In particular, the use of a metal powder and additive manufacturing process is explored for micro-mold inserts, with the purpose of enabling more flexible, customized, and fast mold production without any further post-processing. According to the literature reviews discussed, it can be found that developing a low-cost method to rapidly manufacture a precision mold with micro-features is a current hot research topic. Therefore, in order to demonstrate this capability, molds with different inserts were realized by the L-PBF process, and a set of dogbones and flexural

**Table 14** Economic analysis results

Material	Process	Time (h)	Cost (€)
Steel	EDM	6	390
Hard resin	SLA	6	36
Steel	L-PBF	4	182
Steel	Milling	1	218

hinges made of POM were micro-injected in such a mold. The dogbones were selected for mechanical characterization. The hinges were challenging due to the very thin central part and the consequent cumbersome filling of such cavities, especially during the ejection phase. For this reason, great attention was devoted to mold design, inserts, and assembly. In particular, strategies in cavity designs were applied to meet polymer flow dynamics in thin cavities during the micro-IM process and obtain intact samples. Moreover, careful considerations of the draft angle were made to guarantee the correct ejection of parts threatened by the higher surface roughness of L-PBF molds. To this aim, three and four levels of draft angles were tested for dogbones and hinges, respectively. As a result, it was observed that this parameter did not influence the dogbone production, whereas the hinges failed to be ejected undeformed using a draft angle of  $0.5^\circ$ .

After the fabrication, the dimensional characterization of the mini-dogbones demonstrated a replication accuracy of 3%. At the same time, the hinges showed a deviation from nominal dimensions up to 7%; this fact was caused by the micro-sizes of the central channel and the high volume-to-surface ratio. Also, the mechanical tests evidenced the good performance of the realized samples that reach maximum stress values comparable to those obtained with traditionally manufactured mold.

For the sake of completeness, an evaluation of time and costs for the proposed process chain was reported. In particular, we demonstrated the chance of reducing manufacturing costs from 16 to 50% with respect to conventional milling and electron discharge machining (EDM). In conclusion, L-PBF is quite promising as an efficient alternative for tooling in micro-manufacturing technologies, especially if no particular finishing is required. First, the main advantage of L-PBF molds compared to others realized with polymer-based AM technologies includes their mechanical properties, which make them suitable for longer production cycles. Additionally, using L-PBF and micro-injection molding provides satisfactory mechanical and flexural functionalities for the produced samples.

**Acknowledgements** The authors are grateful to V. Basile, V. Bellantone, V. Marrocco, F. Modica, S.P. Negri, and C. Pagano of STIIMA-CNR for their contribution and helpful discussion.

**Author contribution** All authors contributed to the study conception and design. Material preparation, data collection, and analysis were performed by Rossella Surace, Vito Errico, and Marcello Valori. The first draft of the manuscript was written by Rossella Surace and Vito Errico, and all authors commented on previous versions of the manuscript. All authors read and approved the final manuscript.

**Funding** Open access funding provided by Consiglio Nazionale Delle Ricerche (CNR) within the CRUI-CARE Agreement.

## Declarations

**Competing interests** The authors declare no competing interests.

**Open Access** This article is licensed under a Creative Commons Attribution 4.0 International License, which permits use, sharing, adaptation, distribution and reproduction in any medium or format, as long as you give appropriate credit to the original author(s) and the source, provide a link to the Creative Commons licence, and indicate if changes were made. The images or other third party material in this article are included in the article's Creative Commons licence, unless indicated otherwise in a credit line to the material. If material is not included in the article's Creative Commons licence and your intended use is not permitted by statutory regulation or exceeds the permitted use, you will need to obtain permission directly from the copyright holder. To view a copy of this licence, visit <http://creativecommons.org/licenses/by/4.0/>.

## References

- Vasco JC, Pouzada AS (2013) A study on microinjection moulding using moulding blocks by additive micromanufacturing. *Int J Adv Manuf Technol* 69:2293–2299. <https://doi.org/10.1007/s00170-013-5165-9>
- Pereira T, Kennedy JV, Potgieter J (2019) A comparison of traditional manufacturing vs additive manufacturing, the best method for the job. *Procedia Manuf* 30:11–18. <https://doi.org/10.1016/j.promfg.2019.02.003>
- León-Cabezas MA, Martínez-García A, Varela-Gandía FJ (2017) Innovative advances in additive manufactured moulds for short plastic injection series. *Procedia Manuf* 13:732–737. <https://doi.org/10.1016/j.promfg.2017.09.124>
- ISO/ASTM52900:2015 Additive manufacturing — general principles — Terminology
- Molitch-Hou M (2018) Overview of additive manufacturing process. In: Zhang J, Jung Y-G (eds) *Additive Manufacturing*. Elsevier, pp 1–38
- Mazur M, Brincat P, Leary M et al (2017) Numerical and experimental evaluation of a conformally cooled H13 steel injection mould manufactured with selective laser melting. *Int J Adv Manuf Technol* 93:881–900. <https://doi.org/10.1007/s00170-017-0426-7>
- Han S, Salvatore F, Rech J, Bajolet J (2020) Abrasive flow machining (AFM) finishing of conformal cooling channels created by selective laser melting (SLM). *Precis Eng* 64:20–33. <https://doi.org/10.1016/j.precisioneng.2020.03.006>
- Armillotta A, Baraggi R, Fasoli S (2014) SLM tooling for die casting with conformal cooling channels. *Int J Adv Manuf Technol* 71:573–583. <https://doi.org/10.1007/s00170-013-5523-7>
- Samei J, Asgari H, Pelligra C et al (2021) A hybrid additively manufactured martensitic-maraging stainless steel with superior strength and corrosion resistance for plastic injection molding dies. *Addit Manuf* 45:102068. <https://doi.org/10.1016/j.addma.2021.102068>
- Marin F, de Souza AF, Ahrens CH et al (2021) A new hybrid process combining machining and selective laser melting to manufacture an advanced concept of conformal cooling channels for plastic injection molds. *Int J Adv Manuf Technol* 113:1561–1576. <https://doi.org/10.1007/s00170-021-06720-4>
- Narvan M, Al-Rubaie KS, Elbestawi M (2019) Process-structure-property relationships of AISI H13 tool steel processed with selective laser melting. *Materials (Basel)* 12:1–20. <https://doi.org/10.3390/ma12142284>

12. Kuo CC, You ZY (2018) Development of injection molding tooling with conformal cooling channels fabricated by optimal process parameters. *Int J Adv Manuf Technol* 96:1003–1013. <https://doi.org/10.1007/s00170-018-1664-z>
13. Cunha Â, Marques A, Silva MR et al (2022) Laser powder bed fusion of the steels used in the plastic injection mould industry: a review of the influence of processing parameters on the final properties. *Int J Adv Manuf Technol* 121:4255–4287. <https://doi.org/10.1007/s00170-022-09588-0>
14. Saby Q, Buffière JY, Maire E et al (2021) Laser powder bed fusion printability of cobalt-free steel powders for manufacturing injection molds. *Addit Manuf* 44:102031. <https://doi.org/10.1016/j.addma.2021.102031>
15. Tan C, Wang D, Ma W et al (2020) Design and additive manufacturing of novel conformal cooling molds. *Mater Des* 196:109147. <https://doi.org/10.1016/j.matdes.2020.109147>
16. Sinico M, Ranjan R, Moshiri M et al (2019) A mold case study on topology optimized design for additive manufacturing. 2019 Annu Int Solid Free Fabr Symp – An Addit Manuf Conf 1921–1931
17. Nagarajan B, Hu Z, Song X et al (2019) Development of micro selective laser melting: the state of the art and future perspectives. *Engineering* 5:702–720. <https://doi.org/10.1016/j.eng.2019.07.002>
18. Zhang N, Liu J, Zhang H et al (2019) 3D printing of metallic microstructured mould using selective laser melting for injection moulding of plastic microfluidic devices. *Micromachines* 10:595. <https://doi.org/10.3390/mi10090595>
19. Qian J, Kempen K, Wang J et al (2014) A holistic approach for  $\mu$ EDM milling on SLMed steel. *Conf Proc - 14th Int Conf Eur Soc Precis Eng Nanotechnology, EUSPEN 2014* 2:404–407
20. Schubert A, Zeidler H, Martin A et al (2014) Jet-Electrochemical machining of selective laser melted aluminum and steel alloys for micro injection moulds. *Conf Proc - 14th Int Conf Eur Soc Precis Eng Nanotechnology, EUSPEN 2014* 2:367–370
21. Moshiri M, Loaldi D, Zanini F et al (2021) Analysis of an as-built metal additively manufactured tool cavity insert performance and advantages for plastic injection moulding. *J Manuf Process* 61:369–382. <https://doi.org/10.1016/j.jmapro.2020.11.035>
22. Bellantone V, Surace R, Trotta G, Fassi I (2013) Replication capability of micro injection moulding process for polymeric parts manufacturing. *Int J Adv Manuf Technol* 67:1407–1421. <https://doi.org/10.1007/s00170-012-4577-2>
23. Catoen B, Rees H (2021) *Injection mold design handbook*. Hanser Publications, ISBN-10 156990815X
24. Linß S, Henning S, Zentner L (2019) Modeling and design of flexure hinge-based compliant mechanisms. In: Mizrahi J (ed) *Kinematics - Analysis and Applications*. IntechOpen. <https://doi.org/10.5772/intechopen.85224>
25. Valori M, Surace R, Basile V et al (2020) Rapid fabrication of POM flexure hinges via a combined injection molding and stereolithography approach. Vol 1 14th ASME Int Conf Micro-Nanosyst (MNS). <https://doi.org/10.1115/DETC2020-22476>
26. Campanelli SL, Contuzzi N, Ludovico AD (2010) Manufacturing of 18 Ni Marage 300 steel samples by selective laser melting. *Adv Mater Res* 83–86:850–857. <https://doi.org/10.4028/www.scientific.net/AMR.83-86.850>
27. Lu Y, Wu S, Gan Y et al (2015) Study on the microstructure, mechanical property and residual stress of SLM Inconel-718 alloy manufactured by differing island scanning strategy. *Opt Laser Technol* 75:197–206. <https://doi.org/10.1016/j.optlastec.2015.07.009>
28. Errico V, Fusco A, Campanelli SL (2022) Effect of DED coating and DED + Laser scanning on surface performance of L-PBF stainless steel parts. *Surf Coatings Technol* 429:127965. <https://doi.org/10.1016/j.surfcoat.2021.127965>
29. Bellantone V, Surace R, Fassi I (2022) Quality definition in micro injection molding process by means of surface characterization parameters. *Polymers (Basel)* 14:3775. <https://doi.org/10.3390/polym14183775>
30. Baldi F, Bongiorno A, Fassi I et al (2014) Process–property–structure relationship in miniaturized injection moulded polyoxymethylene samples. *Polym Eng Sci* 54:512–521. <https://doi.org/10.1002/pen.23582>

**Publisher's note** Springer Nature remains neutral with regard to jurisdictional claims in published maps and institutional affiliations.